Building and Environment, Vol. 24, No. 1, pp. 85–97, 1989.
Printed in Great Britain.

0360–1323/89 $3.00 + 0.00

#3331

Numerical and Experimental Study on Room Airflow—3-D Predictions using the k–ε Turbulence Model

SHUZO MURAKAMI*
SHINSUKE KATO*

Accurate prediction of velocity and temperature distributions in a room is indispensable for designing high quality air conditioning systems. This paper is concerned with the feasibility and validity of numerical simulation of room airflow. Turbulent recirculating flows in many types of ventilated rooms were numerically simulated in three-dimensions using the k–ε two equation turbulence model. The results obtained from the numerical simulation are compared with those given by model experiments concerned with velocity and diffusion fields. The correspondence between simulations and experiments is fairly good. It may be concluded that 3-D numerical simulations using the k–ε two equation model can predict turbulent recirculating flows in a ventilated room with sufficient accuracy from the viewpoint of engineering applications.

NOMENCLATURE

C_D, C_1, C_2	empirical constants in turbulence model (*cf.* Table 2)
C	mean contaminant concentration
C_0	representative concentration defined by that of exhaust outlet
k	turbulence kinetic energy
k_0	boundary value for k at inflow
l	length scale of turbulence
l_0	boundary value for l at inflow
L_0	representative length defined by width of supply outlet
P	mean pressure
Re	Reynolds number $Re = U_0L_0/\nu$
U, V, W	X, Y, Z components of velocity vector
U_i, U_j	components of velocity vector
U_0	representative velocity defined by inflow air velocity
y_h	simulation result using mesh size h
ε	turbulence dissipation rate
ε_0	boundary value for ε at inflow
ε_h	solution error of y_h
κ	von Karman constant, 0.4
ρ	fluid density
ν	molecular kinematic viscosity
ν_t	eddy kinematic viscosity
$\sigma_1, \sigma_2, \sigma_3$	turbulence Prandtl/Schmidt number of k, ε, C (*cf.* Table 2)

1. INTRODUCTION

ACCURATE prediction of velocity, temperature and concentration distributions in a room is indispensable for designing high quality air conditioning systems from the viewpoint of such factors as comfort and cleanliness. The major characteristics of airflow in an air conditioned or ventilated room are that it is both turbulent and 3-D. Therefore, the simulation method should be able to predict 3-D turbulent recirculating flows in order to be applicable to engineering problems. Since 3-D simulation requires a large amount of computer storage and computation time, it was impossible in the past to conduct such types of simulations with sufficient accuracy due to the limitations of the computer resources. However, recent advances in computer technology and in numerical methods for fluid dynamics now make it possible to conduct such large scale simulations.

The main objective of this paper is to summarize the problem of 3-D numerical simulation of turbulent airflow in a room (hereafter referred to as turbulent room airflow) and to show the accuracy and validity of simulations. The validity of simulation is confirmed by comparing the simulation with the precise model experiment.

2. ROOM AIRFLOW

For the prediction of room airflow in connection with engineering problems, factors such as the following must be taken into consideration: (i) temperature difference; (ii) room shape; (iii) flow obstacles; (iv) turbulence model; (v) numerical method. As stated above, the main purpose of this paper is to show the validity of 3-D numerical simulation for turbulent room airflow. Therefore, the simulations dealt with in this paper are performed under rather simplified conditions. The air temperature field is assumed to be uniform and the buoyancy effect is not incorporated. Simply shaped rooms are chosen as models, and simulations are conducted by the finite difference method using rectangular meshes. The effect of buoyancy can be dealt with by using more complex turbulence modelling and simulation with rooms of complicated shape can be treated by the boundary fitted coordinate methods. Both will be discussed in a future paper.

* Institute of Industrial Science, University of Tokyo, Japan.

Table 1. Specifications of room models

Room type	Dimension on plan*	Height of ceiling*	Number of outlets	Number of inlets	Supply velocity†	Remarks
Type 1	5 × 5	4.5	1	4	1.0	smallest room
Type 2	8 × 8	4.5	4	4	1.0	w./w.o. obstacle
Type 3	11 × 11	4.5	9	4	1.0	largest room

* Dimensionless value: all lengths have been made dimensionless by means of the width of the supply outlet.
† Dimensionless value: all velocities have been made dimensionless by means of the inflow velocity.

Recirculating flow in a room is usually turbulent. However, sometimes it is not fully turbulent [1], i.e. where the flow pattern is dependent on the Reynolds number. If the flow pattern in a room changes according to the Reynolds number, the turbulence model must make provision for it. Since room airflows are assumed here to be fully turbulent, the basic equations of the turbulence models are derived on the basis of an assumption of fully developed turbulence. Simulations based on the low Reynolds number modelling method will not be discussed here.

In this paper, airflows in conventional turbulent flow type clean rooms are simulated. As the rate of exchange of air in a clean room is very large, the flow can be expected to be highly turbulent and the temperature field almost uniform. Moreover, severe regulation of airflow distribution in a clean room is essential because of the necessity for quality control. From these points of view, a clean room may be regarded as one of the most appropriate environments for studying techniques of turbulent flow simulation.

Three types of room models are treated in this paper. The specifications of each room model are presented in Table 1. Figure 1 shows the geometry of each room model.

In this study, physical quantities are made dimensionless by dividing by representative quantities. These quantities are the width of the supply outlet L_0 and its bulk velocity U_0. The ceiling height of all types of room models is 4.5 in dimensionless value; this means that a jet from the ceiling outlet reaches the floor before it grows into a fully developed, self-preserving turbulent jet because the distance between the floor and ceiling is only 4.5 times L_0. The openings of the supply outlet and the exhaust inlet have the same shape.

3. MODEL EXPERIMENT

3.1. *Model*

Room models, 1/6 of full scale, are used for experiments. The representative length, that is, the width of the supply outlet L_0, is set as 0.1 m in the models. The ceiling height of all types of room models is 0.45 m, which would be 2.7 m in a full scale room. The representative velocity, the velocity of the jet from the supply outlet U_0, is set at about 6 m s^{-1}. The Reynolds number of the inflow jet U_0L_0/ν is about 4.2×10^4. The velocity of the jet from the supply outlet in full scale conventional clean rooms is usually set at about 1 m s^{-1} for filtering efficiency. Therefore, the Reynolds number for the model experiment approximately corresponds to that for a full scale clean room. The room models used are shown in Fig. 1. Not only the air volume rate, but also the velocity distributions both at the outlet and inlet are carefully adjusted so that the degree of scatter in the measured values of U_0 falls within $\pm 7\%$ of the respective average values.

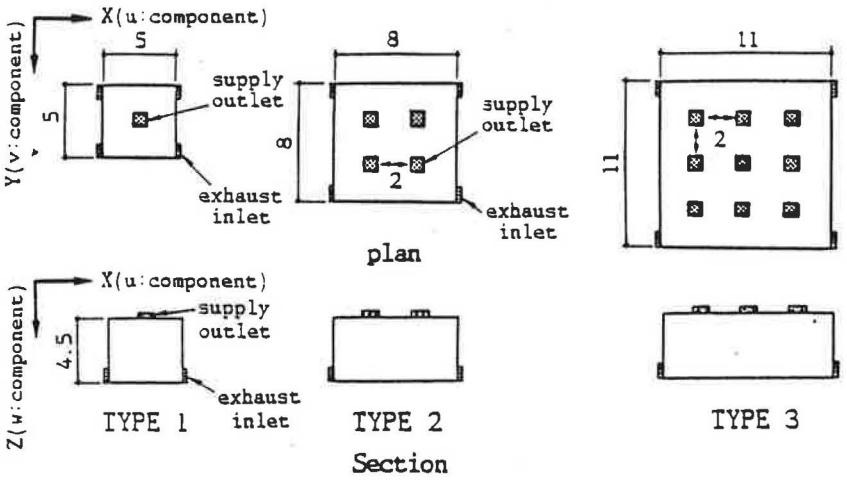

Fig. 1. Plans and section of model clean rooms. (Length scale in this figure is non-dimensionalized by the width of the supply outlet L_0.)

3.2. *Measurement of air velocity and gas concentration*

Air velocity is measured by means of a tandem-type, parallel hot wire anemometer which can discern the vector components of turbulent flow [2].

The airflow in the room model is also visualized. The flow visualization is conducted with a laser light sheet system [3]. The laser light beam (Argon ion laser, 4 W) is dispersed into a light sheet by the cylindrical lens. Magnesium carbonate ($MgCO_3$) powder (1 to 10 μm) is used as the tracer.

The mechanism of passive scalar diffusion is investigated by means of a tracer gas diffusion experiment. Ethene (C_2H_4) is used for the tracer and its concentration is measured by means of F.I.D. gas chromatography.

4. NUMERICAL SIMULATION

The accuracy of numerical simulation depends on both the numerical scheme and the mesh resolution. The mesh resolution required for accurate simulation is related to the local characteristic scale of turbulent flow as well as the properties of the numerical scheme. In no case can numerical simulation eliminate errors caused by deficiencies in the turbulence model or errors arising from the numerical method. Since all numerical schemes have second order accuracy, and since a sufficiently fine mesh system is used in this paper, discrepancies between the simulations and the experiments may be regarded as caused mainly by deficiencies in the turbulence modelling.

4.1. *Methods of simulating turbulent flows*

There are many methods for simulating turbulent flow. The three major categories are listed below.

(1) Reynolds-averaged equations. In this method, Navier–Stokes equations which govern fluid motion are averaged either over time or an ensemble of essentially equivalent flows. The equations describing the mean field are the fundamental equations of computer simulation. The averaging process of the Navier–Stokes equation includes the unknown averages of the products of fluctuating velocities, one of which is the well-known Reynolds stress. These unknown correlation terms must be approximated by the known terms, and the closed set of fundamental equations is required. Of such sets of equations, one of the most well known is the k–ε two equation model of turbulence.

(2) Large eddy simulation. In this approach, Navier–Stokes equations are averaged over a small spatial region. This method enables the simulation of a fluctuating turbulent flow field.

(3) Full simulation. This is the numerical solution of the exact Navier–Stokes equation. The length scale of turbulence motion is usually very small; in a flow field in a room, this scale is less than 0.1 mm. Thus, this method requires a very fine mesh system and is therefore difficult to apply to the analysis of room airflow.

From the viewpoint of engineering use, simulation based on the Reynolds averaged equation is the most efficient and commonly used. The k–ε two equation model is used to incorporate the effect of turbulence on the flow. The model was first developed by Harlow and Nakayama [4] and further refined by Launder and Spalding [5]. The equations of the k–ε model [4] are given in Table 2. Equation (6) in Table 2 is a transport equation for passive contaminants. The source term in Equation (6) is omitted, as its value is always zero except at the source point.

This model has been widely applied in predicting many types of turbulent flow phenomena. Two dimensional room airflow simulation based on the k–ε model was first conducted by Nielsen [6]. However, only a few studies, such as the works of Sakamoto and Matsuo [7], Nomura *et al.* [8] and Murakami *et al.* [9] have been conducted to examine the accuracy of numerical simulation for 3-D recirculating flow in a ventilated room. There have also been very few studies in which the distribution of air velocity was measured in detail, although air flow in a ventilated room is a very common physical phenomenon. Only by such detailed experiments can the accuracy of the results of 3-D numerical simulation be examined.

Table 2. Model equations (two equation of k–ε type)

$\dfrac{\partial U_i}{\partial X_i} = 0$	(1) Continuity equation.
$\dfrac{\partial U_i}{\partial t} + \dfrac{\partial U_i U_j}{\partial X_j} = -\dfrac{\partial}{\partial X_i}\left(\dfrac{P}{\rho} + \dfrac{2}{3}k\right) + \dfrac{\partial}{\partial X_j}\left[\nu_t \left\{\dfrac{\partial U_i}{\partial X_j} + \dfrac{\partial U_j}{\partial X_i}\right\}\right]$	(2) Momentum equations.
$\dfrac{\partial k}{\partial t} + \dfrac{\partial k U_j}{\partial X_j} = \dfrac{\partial}{\partial X_j}\left\{\dfrac{\nu_t}{\sigma_1}\dfrac{\partial k}{\partial X_j}\right\} + \nu_t S - \varepsilon$	(3) Transport equation for k.
$\dfrac{\partial \varepsilon}{\partial t} + \dfrac{\partial \varepsilon U_j}{\partial X_j} = \dfrac{\partial}{\partial X_j}\left\{\dfrac{\nu_t}{\sigma_2}\dfrac{\partial \varepsilon}{\partial X_j}\right\} + C_1 \dfrac{\varepsilon}{k}\nu_t S - C_2 \dfrac{\varepsilon^2}{k}$	(4) Transport equation for ε.
$\nu_t = k^{1/2} l = \left\{C_D \dfrac{k^2}{\varepsilon}\right\}$	(5) Equation for deciding ν_t.
$\dfrac{\partial C}{\partial t} + \dfrac{\partial C U_j}{\partial X_j} = \dfrac{\partial}{\partial X_j}\left\{\dfrac{\nu_t}{\sigma_3}\dfrac{\partial C}{\partial X_j}\right\}$	(6) Concentration equation.
Here : $S = \left\{\dfrac{\partial U_i}{\partial X_j} + \dfrac{\partial U_j}{\partial X_i}\right\}\dfrac{\partial U_i}{\partial X_j}$, $\sigma_1 = 1.0$, $\sigma_2 = 1.3$, $\sigma_3 = 1.0$ $C_0 = 0.09, C_1 = 1.44, C_2 = 1.92$.	

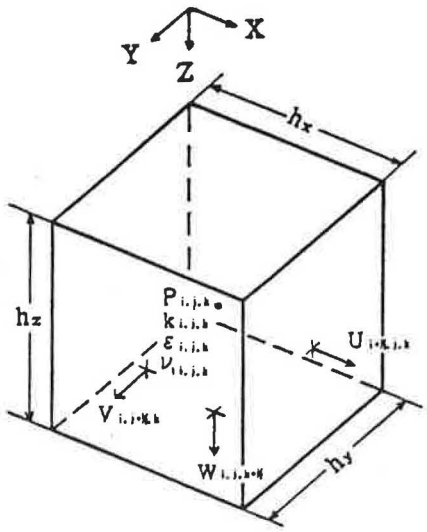

Fig. 2. Definition points of velocity components and scalar quantities.

Numerical simulation of room airflow based on LES (Large Eddy Simulation) was first conducted by Sakamoto and Matsuo [7]. Hibi *et al.* [10] and Murakami *et al.* [11] have examined the accuracy of numerical simulation based on LES for 3-D recirculating flow. Because LES reproduces the fluctuating velocity field, and because it is difficult to measure the 3-D turbulence properties in an experiment, examining the correspondence between simulation and experiment is an arduous task. Simulation with LES will not be discussed here.

4.2. *Numerical methods*

A staggered mesh system is adopted as shown in Fig. 2. The definition points of the variables are the same as those in the usual marker-and-cell (MAC) method [12]. Velocity components are defined at the centre of the cell surfaces and scalar quantities are set in the centre of the cell as shown in Fig. 2. For momentum equations, the centred difference scheme is adopted for both the convective terms as well as other terms. The QUICK (Quadratic Upstream Interpolation for Convective Kinematics) scheme [13], a second order up-wind scheme for convective terms, is partially adopted only near the exhaust inlets in order to remove the spatial oscillation caused by numerical instability. For transport equations of scalar quantities (k, ε and C), the QUICK scheme is adopted. Thus, all spatial derivatives are approximated by second order finite difference schemes. For discretization in time, the Adams–Bashforth method is used. Numerical integration is conducted following the ABMAC method, a simultaneous iterative method for pressures and velocities [14, 15]. Stationary solutions are obtained.

4.3. *Mesh system and error estimation*

The mesh systems used are shown in Fig. 3. In order to examine the influence of mesh resolution on the results of calculations, preliminary numerical simulations based on various coarse mesh systems were conducted and the results were compared with the experimental data. Figure 4 shows the results of a model experiment of Type 2, and Fig. 5 shows the results of preliminary simulations which used the boundary conditions given in Table 3. As is shown in Figs 5a and b, when the mesh resolution is coarse, a rising stream between the jets near the floor is not reproduced. The results obtained when using the fine mesh (Fig. 5b) correspond well with those of the experiment (Fig. 4a).

Errors arising from the finite difference method can be well estimated by the solution error given by the Richardson-estimated extrapolation [16]. This method assumes that the solution error can be expressed as a Taylor series. If the finite difference scheme has second order accuracy, a solution error ε_h, of mesh size h can be estimated using both y_h, the solution of mesh size h, and

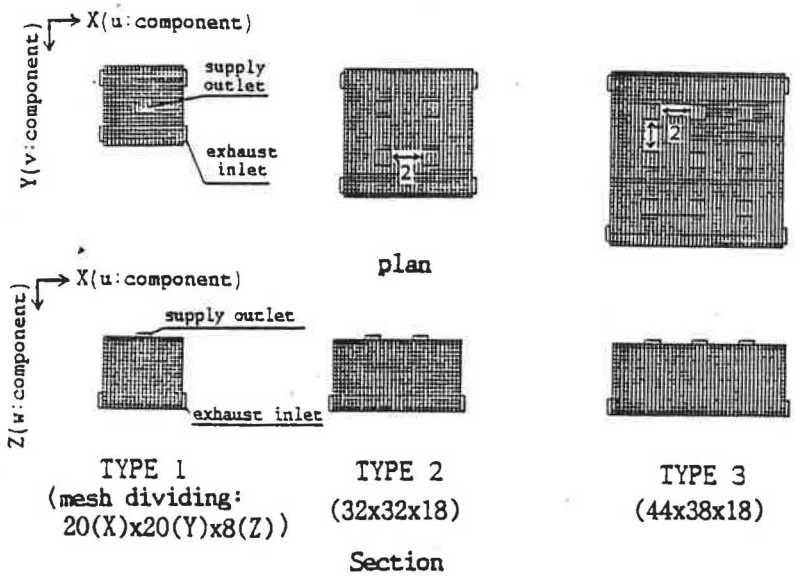

Fig. 3. Mesh systems.

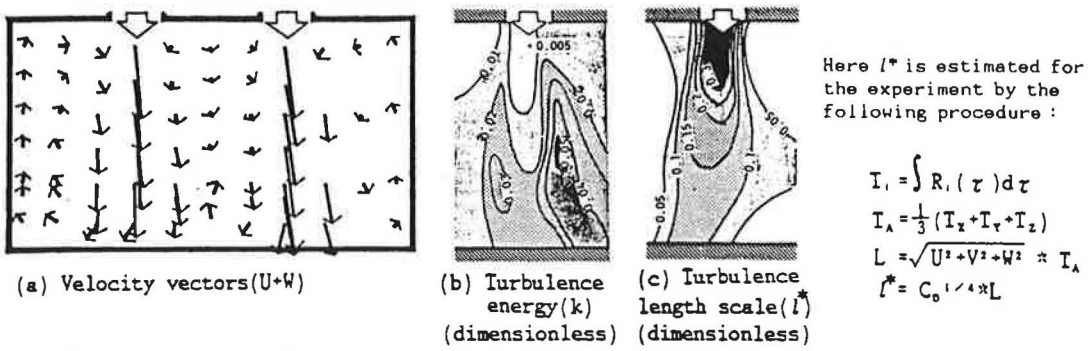

Fig. 4. Results of experiment in case of Type 2. (Vertical section including supply outlets.)

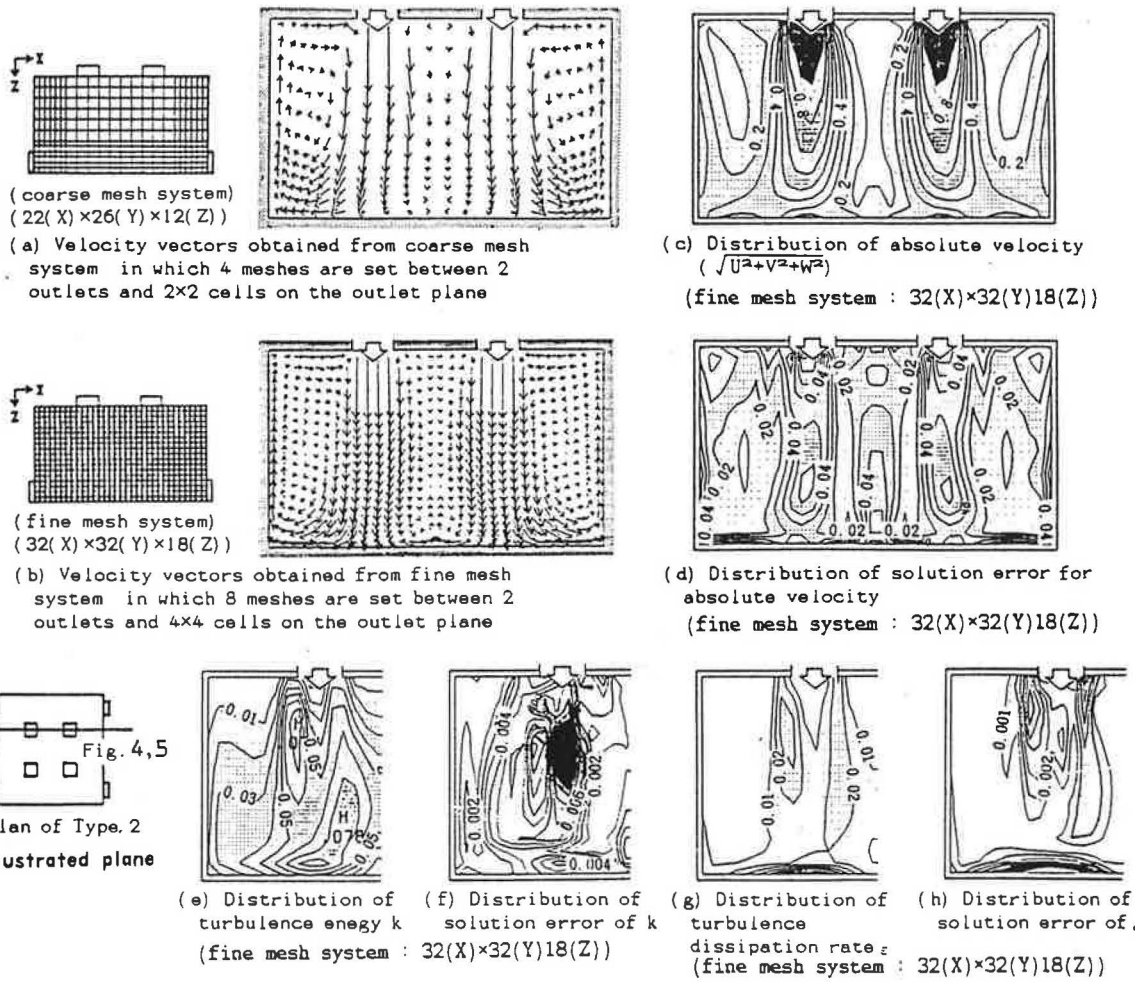

Fig. 5. Comparisons of simulation based on different mesh systems (Type 2).

Table 3. Boundary conditions

(1) Supply outlet boundary	$U_t = 0.0$, $U_n = U_{out}$, $k = 0.005$, $l = 0.33$, $C = 0.0$; suffix t: tangential component, n: normal component, U_{out}: supply outlet velocity, $U_{out} = 1.0$.
(2) Exhaust inlet boundary:	$U_t = 0.0$, $U_n = U_{in}$, $\partial k/\partial Z = 0.0$, $\partial \varepsilon/\partial Z = 0.0$, $\partial C/\partial Z = 0.0$, U_{in}: exhaust inlet velocity, in case of Type 2: $U_{in} = 1.0$.
(3) Wall boundary:	$\partial U/\partial Z_{z=0} = mU_{t_{z=h}}/h$, $U_n = 0.0$, $\partial k/\partial Z = 0.0$, $\partial C/\partial Z = 0.0$, $\varepsilon_{z=h} = [C_D k_{z=h}^{3/2}]/[C_D^{1/4}\kappa h]$, h: length from the wall surface to the centre of the adjacent cell; m: 1/7, Power law of profile $U_t \propto Z^m$ is assumed here; κ: 0.4, von Karman constant.

y_{2h}, that of mesh size $2h$, as follows:

$$\varepsilon_h = (y_h - y_{2h})/3. \quad (7)$$

The distribution of the solution error is calculated at all mesh points using Equation (7).

Figure 5c shows the contour lines of the resultant velocity obtained by using a fine mesh. Figure 5d shows the distribution of the solution error of the resultant velocity. As is shown in Figs 5c and d, the solution error is kept below about one-tenth of the resultant velocity in the whole space. Figure 5e shows the contour lines of the turbulence energy and Fig. 5f the estimation of solution error. The simulated distribution of turbulence energy corresponds well with the experiment and has minimal solution errors. Figures 5g and h show, respectively, the contour lines of the turbulence dissipation rate and the estimation of the solution error, the latter being kept to a small value.

On the basis of the above analyses, the mesh systems shown in Fig. 3 are adopted in these cases.

4.4. *Boundary conditions*

The boundary conditions for rigid walls, tabulated in Table 3, are assumed as follows.

(1) Velocity component normal to the wall is zero at the wall. Shear stress at the wall, which is required to solve the momentum equation, is derived from the assumption that the profile of tangential air velocity near the wall obeys the distribution expressed as $U(z) \propto z^m$, $m = 1/7$.

(2) The gradient of turbulence energy k normal to the wall is zero, i.e. $\partial k/\partial z = 0$.

(3) The length scale of turbulence l is proportional to the distance from the wall, namely, $l(z) = C_D^{1/4}\kappa z$. (Here, z denotes the coordinate normal to the wall.)

The boundary conditions for inflows are given as follows.

(1) Uniform velocity distribution is assumed over the supply outlets.

(2) Uniform distributions of k and ε are also assumed over the supply outlets. The values k and ε used in these simulations are chosen according to the values obtained from measurements ($k_0 = 0.005$, $l_0 = 0.33$, $\varepsilon_0 = C_D k_0^{3/2}/l_0$).

The boundary conditions for outflows are assumed as follows.

(1) Uniform velocity distribution is assumed over the exhaust inlets.

(2) The gradients of k, ε and C normal to the exhaust inlets are zero.

5. NUMERICAL SIMULATION AND COMPARISON WITH EXPERIMENT

5.1. *Type* 1

The distributions of velocity vectors in several of the sectional planes are compared in Fig. 6. The correspondence between simulations and experiment is good. The mean flow pattern of Type 1 is summarized as follows: (i) the air jet from the supply outlet at the ceiling reaches the floor without a decrease in velocity; (ii) the jet stream hits the floor and diverges toward the wall; (iii) the diverged streams reach the walls and turn up toward the ceiling—thin and strong rising streams are observed along the walls to the ceiling; (iv) after the rising wall-streams arrive at the ceiling and converge toward the centre, they are induced into the jet of the supply outlet.

Not only the main recirculating flow but also the second flows are well reproduced by this numerical simulation.

5.2. *Type* 2 *without obstacles in the room*

The distributions of velocity vectors in several of the sectional planes are compared in Figs 7 and 8. Many aspects of the flow pattern of Type 2 are similar to those of Type 1. It may be reasonable, in modelling, to regard the flow pattern of Type 2 as a combination of the four flow patterns of Type 1. In the Type 2 model room, not only the main recirculating flow but also the secondary flows are well reproduced by numerical simulation.

5.3. *Type* 2 *with obstacles in the room*

Flow obstacles in a room affect the flow field of the room. In Fig. 9, the distributions of velocity vectors in a room, where a table is beneath the supply outlet, are shown. The air jet from the supply outlet impinges on the table and diverges to the left and the right. The flow diverging to the right turns downward at the edge of the table and is induced into the flow which streams from the right to the left along the floor. The flow diverging to the left reaches the wall and rises along it to the ceiling. The jet from the right supply outlet and its recirculating flow are hardly affected by the table. Not only the main recirculating flow but also the secondary flows are well reproduced by this simulation.

In the case shown in Fig. 10, the box is arranged on the floor so that it is in contact with the wall. The strong rising streams are observed just to the right of the box and there is a downward flowing stream along the wall over the box. The flow field is greatly affected by the box. The correspondence between simulation and experiment is fairly good.

5.4. *Turbulence characteristics in Type* 2

The advantage of numerical simulation is its ability to analyse the turbulence characteristics of the flow field. Even the most expensive and elaborate measuring instruments hardly allow one to analyse the minute characteristics of the turbulent flow field. As is shown in Fig. 11, one can easily analyse the turbulence properties in the flow field by numerical simulation.

As shown in Fig. 11a, the major part of the mean momentum energy exists in the supply jet. The distribution of turbulence kinetic energy is shown in Fig. 11b, and the turbulence energy production rate is shown in Fig. 11c. From these figures, it is seen that both quantities are very high at the mixing layer around the jets. In Fig. 11d, the distribution of turbulence dissipation rate is shown. It is seen to have a high value not only at the

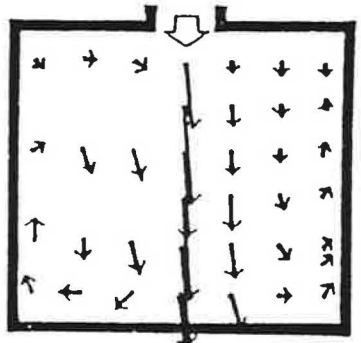

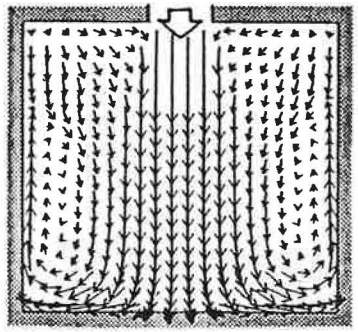

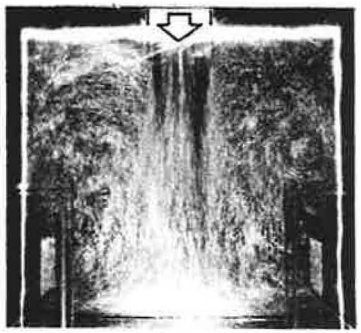

(a) Center of room.

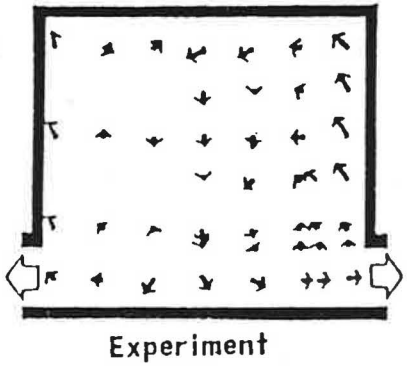

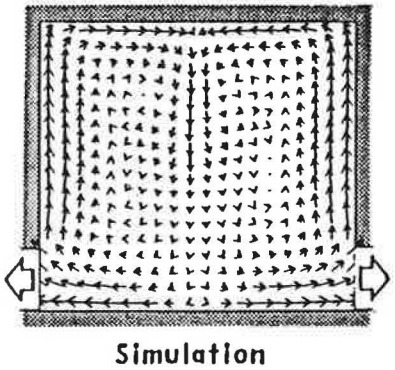

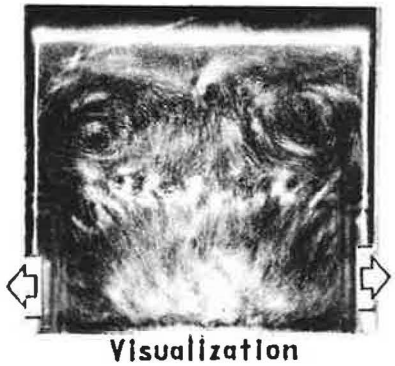

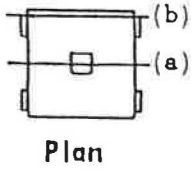

(b) Near wall.

(vector length of supply outlet velocity: ⟶)

Fig. 6. Comparisons of velocity vectors in Type 1 room model (vertical section)

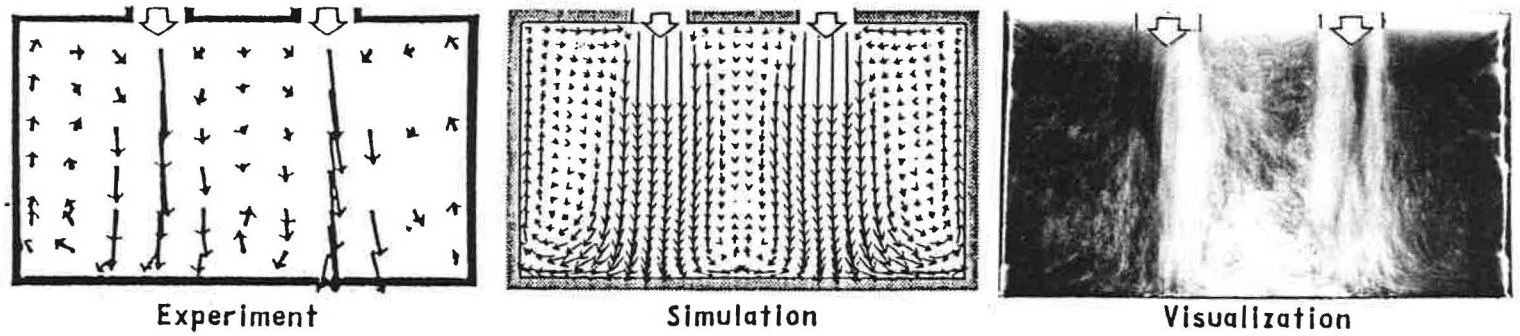

(a) Including supply outlets.

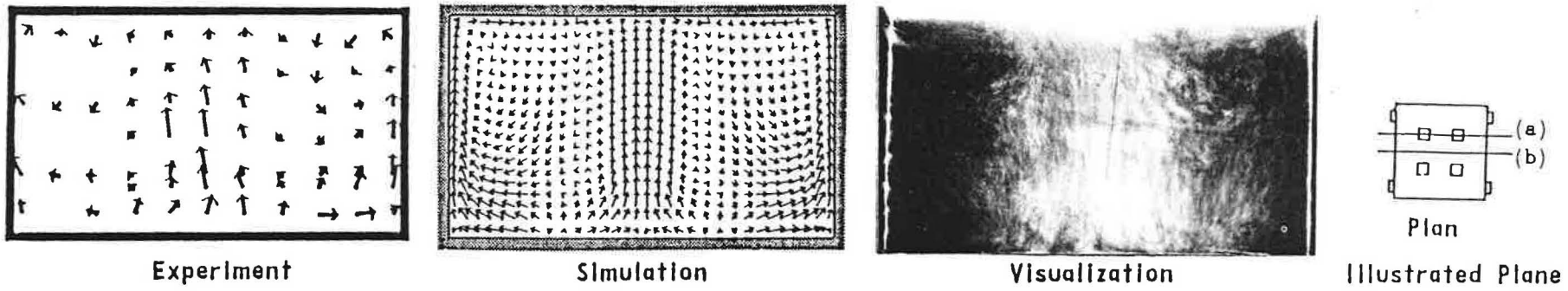

(b) Center of room.

(vector length of supply outlet velocity: ⟶)

Fig. 7. Comparisons of velocity vectors in Type 2 room model (vertical section).

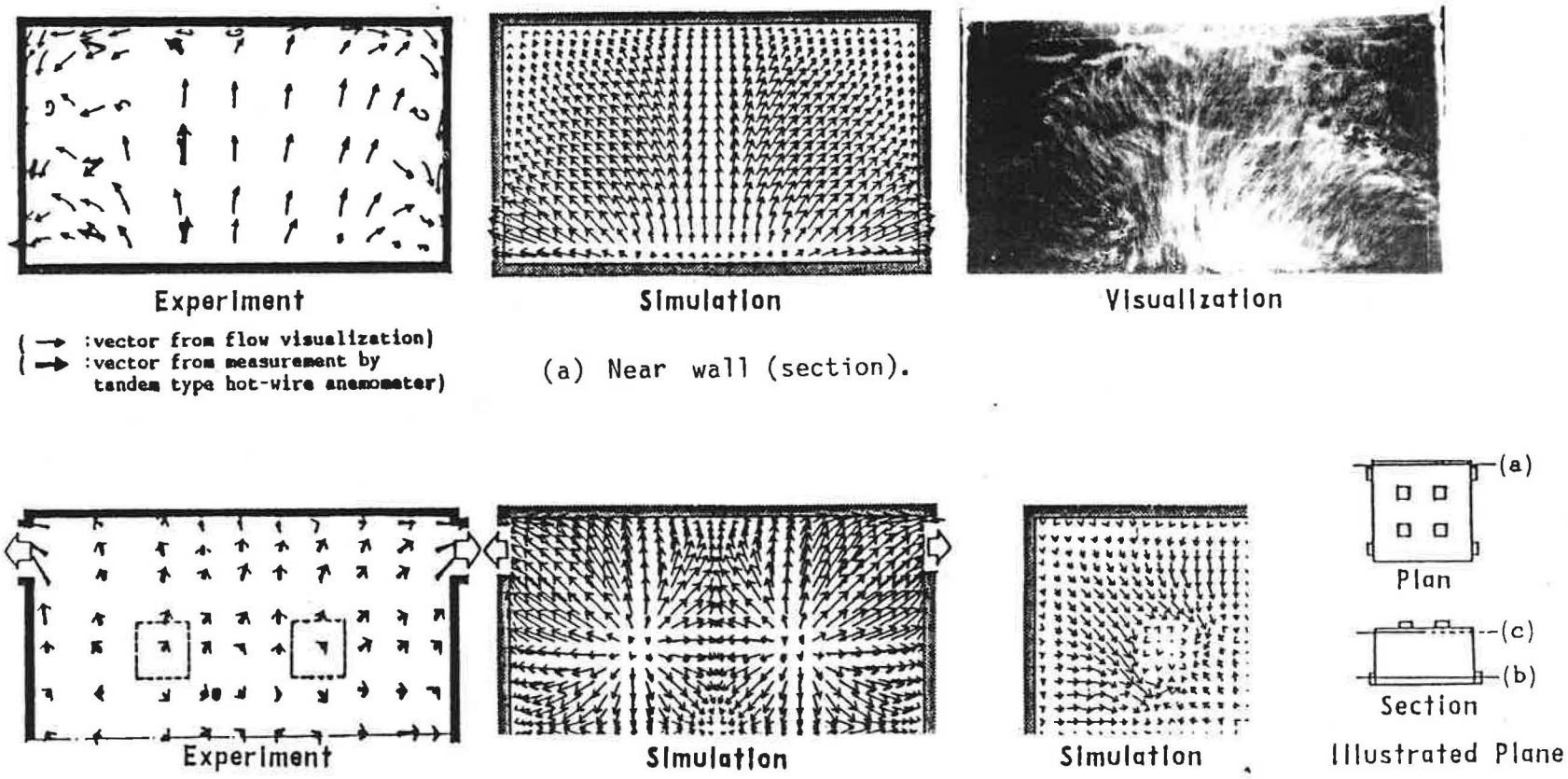

Fig. 8. Comparisons of velocity vectors in Type 2 room model (vertical section and horizontal plane).

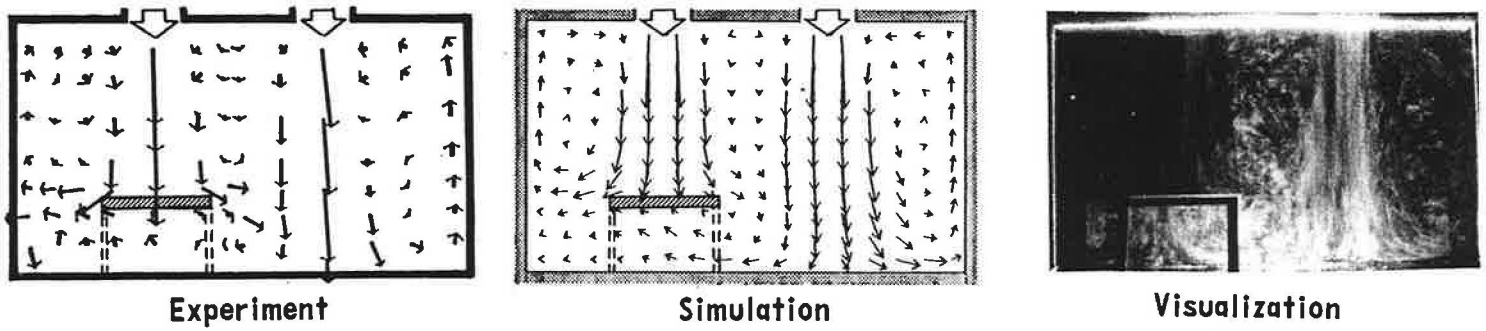

(a) Flow field with obstacle beneath supply outlet

Fig. 9. Velocity vectors in Type 2 with a table (flow field with obstacle beneath supply outlet).

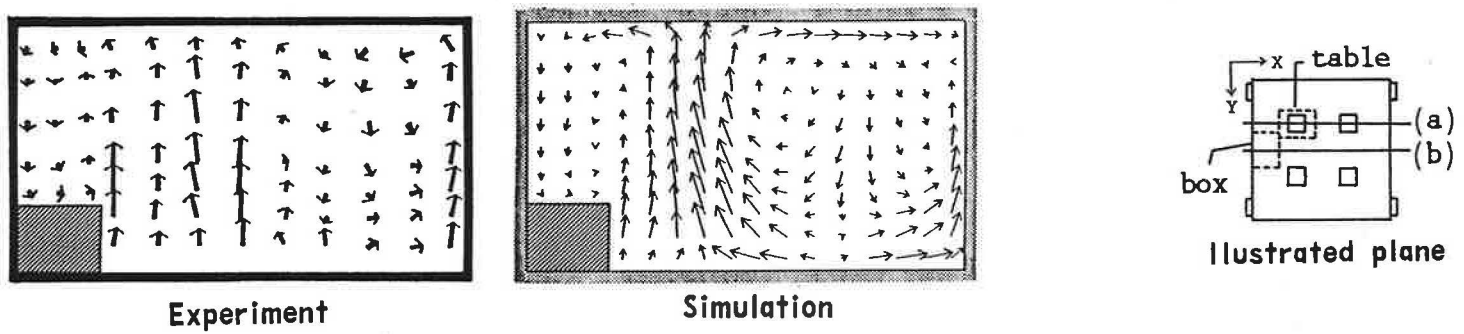

Fig. 10. Velocity vectors in Type 2 with box (flow field with obstacle in contact with wall).

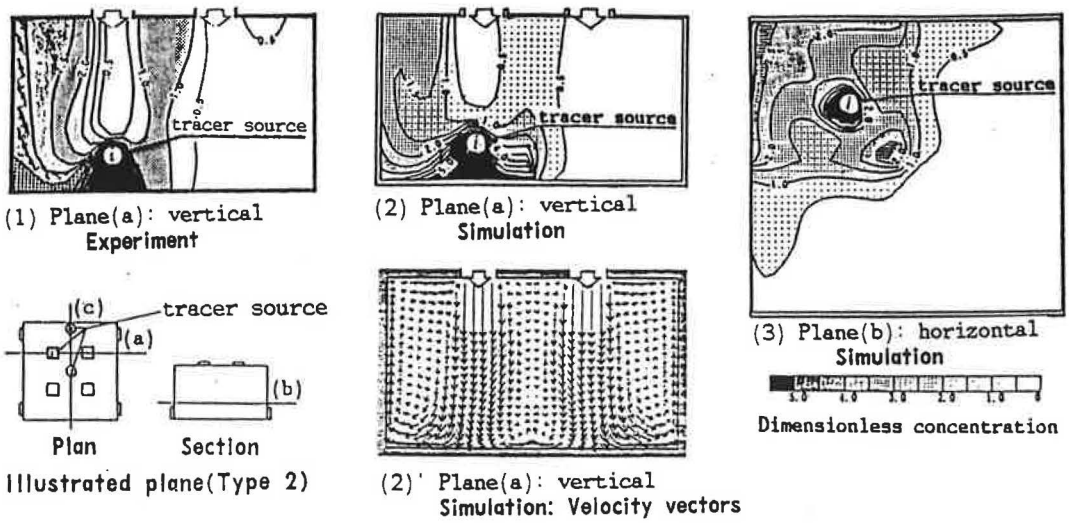

Fig. 13. Comparison of contaminant distribution (source: point *i*).

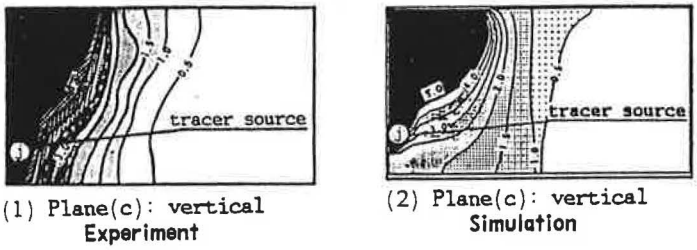

Fig. 14. Comparison of contaminant distribution (source: point *j*).

models, the main recirculating flow is well reproduced by the numerical simulation, as are the small vortices. The distribution of velocity vectors in the plan, where measurements of velocity was not conducted, is also shown to facilitate understanding of the entire flow field. The correspondence between the numerical simulations and the experiments is very close.

6. NUMERICAL PREDICTION FOR CONTAMINANT CONCENTRATION

The distributions of passive scalar contaminants (airborne particles or gaseous contaminants) for simulations and experiments are compared using the Type 2 room model. Comparisons are made for two different positions of the tracer source. The contaminant concentrations of both the experiments and the simulations are normalized by the concentration of the exhaust outlet. Figure 13 shows a comparison of the distribution of contaminant concentration in the case where the tracer source is located at point *i*. The distribution given by the numerical simulation corresponds well with the experimental data. Although the contour lines of concentration are not exactly the same, the main characteristics of the contaminant diffusion are well reproduced: the shape of the high concentration region under the tracer source, the low concentration region under the supply outlet and the low concentration area of the opposite side where no tracer source exists.

Figure 14 shows comparisons of the distribution of contaminant concentration in the case where the tracer source is located at point *j*. As the contaminant is transported mostly by the main airflow, the high concentration region spreads from the tracer source along the main flow direction. While the contour lines of the simulated concentration do not correspond as well as those in Fig. 13, the main characteristics of the contaminant diffusion are generally the same.

From the viewpoint of engineering applications, it may thus be concluded that numerical simulation can be successfully used for the prediction of contaminant diffusion.

7. DISCUSSION

The correspondence between the numerical simulations and the experiments is rather close. Numerical simulation of turbulent flow has thus been proven to be a fairly promising tool for analysing turbulent airflow in a conventional flow type clean room. It not only allows one to analyse the flow field quantitatively, but also to easily analyse the various cases of contaminant diffusion with various locations of the contaminant sources.

However, it must be noted that the comparisons given here between the simulations and the experiments are limited to the mean velocity field. Further research on turbulence properties must be conducted in order to verify the validity of turbulence modelling. In particular, measuring such turbulence properties as the Reynolds stress and the turbulence dissipation rate is extremely difficult for a 3-D recirculating flow. Furthermore, it

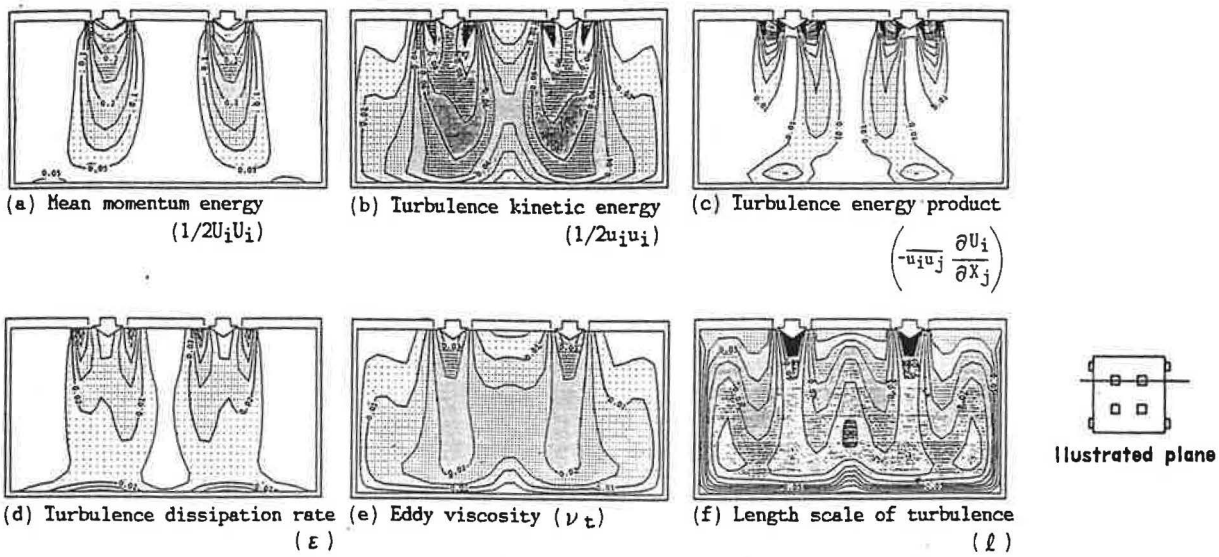

Fig. 11. Turbulence characteristics of simulated flow field in Type 2.

mixing layer of the jets, but also at the impinging region of the jets on the floor.

From the viewpoint of mesh dividing, turbulence energy, production and dissipation have large values at the boundary of the supply jets where mixing with the atmosphere occurs. To consider the rapid changes in these values properly, a fine mesh system is required.

In Fig. 11e, the distribution of turbulence kinematic viscosity is shown. The viscosity is high in and around the supply jet. In Fig. 11f, the distribution of turbulence length scale is shown. It distributes more uniformly than the other turbulence properties.

5.5. *Type* 3

Figure 12 shows a comparison of velocity vectors in the Type 3 room model. As in the other types of room

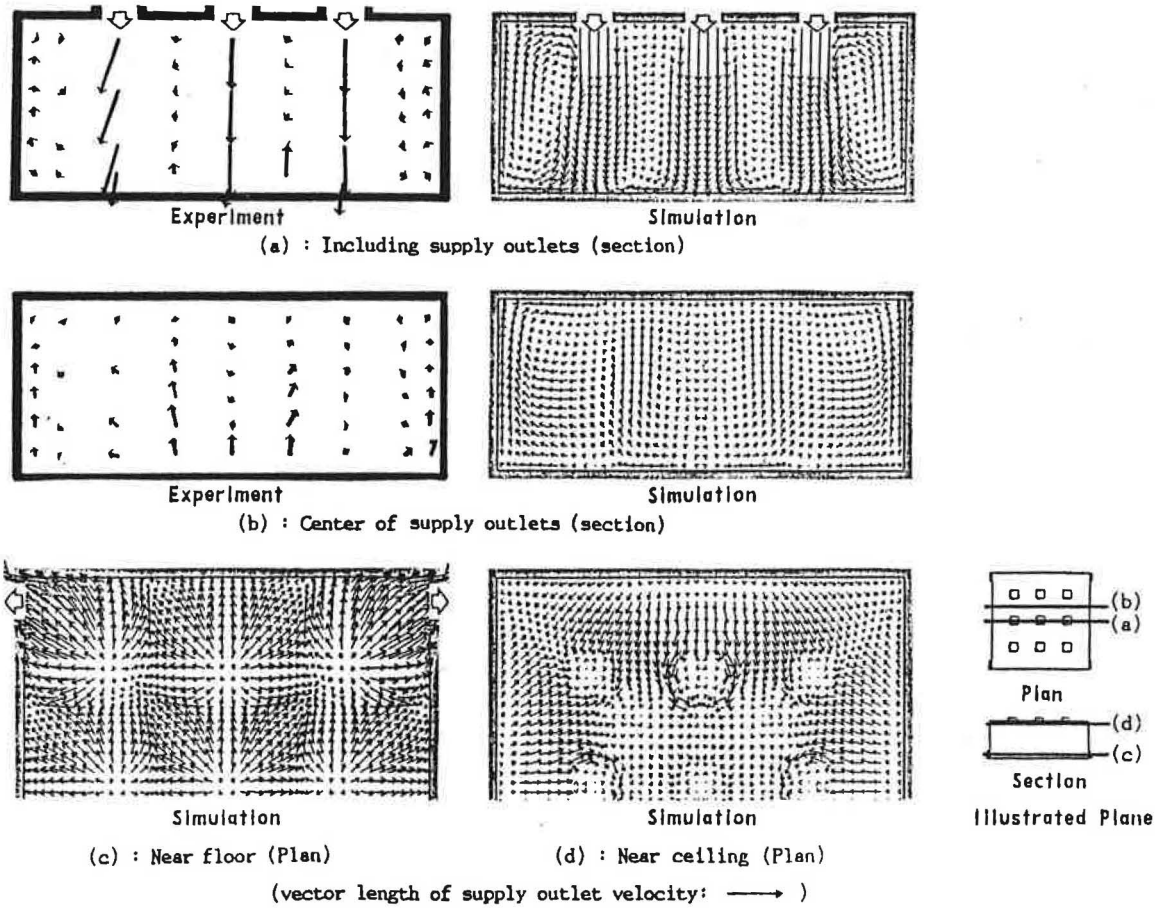

Fig. 12. Comparisons of velocity vectors in Type 3 room model.

must be noted that only highly turbulent flows in which viscosity effects are neglected are simulated in this study. If the airflow in a room cannot be assumed to be fully turbulent, a simulation based on the present turbulence model cannot always be expected to reproduce the flow field with sufficient accuracy.

8. CONCLUSIONS

Numerical simulations of the 3-D turbulent recirculating flow in rooms were compared with precise model experiments. Furthermore, the accuracy of the numerical simulation of the 3-D turbulent recirculating flows was examined. Comparison between the simulations and the experiments was conducted on the following basis.

(1) The airflow simulated in this study was assumed as follows: (i) the airflow was fully turbulent and 3-D; (ii) the temperature of the flow field was uniform; (iii) simply shaped room models were used.

(2) The numerical scheme which was used to solve the k–ε model equations had second order accuracy, and sufficiently fine mesh systems were used.

(3) The solution error arising from the numerical method was estimated by the Richardson extrapolation. The solution error of this simulation was sufficiently small from the viewpoint of practical application.

(4) Precise model experiments were conducted. The 3-D recirculating flow was measured three-dimensionally by means of the special parallel hot wire anemometer. Flow visualization was conducted by means of the laser light sheet method which enables comprehension of the entire flow field.

(5) Correspondence in the mean velocity field between the simulations and the experiments was very close.

Thus, it was confirmed that numerical simulation of the 3-D turbulent recirculating flow in a ventilated room by means of a k–ε model corresponds well with the experimental result. Numerical prediction of room airflow was proven to be a very promising technique.

REFERENCES

1. S. Murakami, T. Tanaka and S. Kato, Numerical simulation of air flow and gas diffusion in room model. Proceedings the Fourth International Symposium on the Use of Computers for Environmental Engineering Related to Buildings, Tokyo (1983).
2. S. Murakami and H. Komine, Measurement of three components of turbulent flow with tandem hot-wire probe. *Trans. Archit. Inst. Jpn* **297**, 59–69 (1980).
3. S. Murakami, S. Kato and S. Akabayashi, Visualization with laser light sheet applied to internal and external air flows in building environmental engineering, in *Fluid Control and Measurement*, pp. 691–696. Pergamon Press, Oxford (1985).
4. F. H. Harlow and P. I. Nakayama, Turbulence transport equation. *Phys. Fluids* **10**, 2323–2332 (1967).
5. B. E. Launder and D. B. Spalding, *Mathematical Models of Turbulence*. Academic Press, London (1972).
6. P. V. Nielsen, Prediction of temperature and velocity distribution in an air-conditioned room. Proceedings of the Second Symposium on the Use of Computers for Environmental Engineering Related to Buildings, Paris (1974).
7. Y. Sakamoto and Y. Matsuo, Numerical predictions of three-dimensional flow in a ventilated room using turbulence models. *Appl. Math. Modelling* **4**, 67–72 (1980).
8. T. Nomura, S. Murakami, S. Kato and M. Sato, Correspondence of the three-dimensional numerical analysis of turbulence flow to model experiment. *Trans. Archit. Inst. Jpn* **298**, 69–80 (1980).
9. S. Murakami, S. Kato and Y. Suyama, Three-dimensional numerical simulation of turbulent air flow in ventilated room by means of two-equation model. *ASHRAE Trans.* **93** (2) (1987).
10. K. Hibi, S. Murakami and A. Mochida, Prediction of room air flow by means of large eddy simulation. Summaries of Technical Papers of Annual Meeting, Architectural Institute of Japan (1985).
11. S. Murakami, A. Mochida and K. Hibi, 3-D numerical simulation of room convection by means of large eddy simulation. Technical Display for NBS/CBT Building Technology Symposium, Room Convection and Indoor Air Quality Simulation Modelling, NBS Administration Building, Gaithersburg, Maryland (1986).
12. F. H. Harlow and J. E. Welch, Numerical calculation of time-dependent viscous incompressible flow of fluid with free surface. *Phys. Fluids* **8**, 2182–2189 (1965).
13. B. P. Leonard, A stable and accurate convection modelling procedure based on quadratic upstream interpolation. *Comput. Methods Appl. Mech. Engng* **19**, 59–98 (1979).
14. J. A. Viecelli, A computing method for incompressible flows bounded by moving walls. *J. Comput. Phys.* **8**, 119–143 (1971).
15. C. W. Hirt and J. L. Cook. Calculating three-dimensional flows around structures and over rough terrain. *J. Comput. Phys.* **10**, 324–340 (1972).
16. S. C. Caruso, J. H. Ferziger and J. Oliger, Adaptive grid techniques for elliptic fluid flow problems. AIAA 24th Aerospace Sciences Meeting, Reno, Nevada (1986).